J Fusion Energ (2012) 31:357–367
DOI 10.1007/s10894-011-9473-5

ORIGINAL RESEARCH

The $^{11}B(p,\alpha)^{8}Be \rightarrow \alpha + \alpha$ and the $^{11}B(\alpha,\alpha)^{11}B$ Reactions at Energies Below 5.4 MeV

M. C. Spraker · M. W. Ahmed · M. A. Blackston · N. Brown · R. H. France III · S. S. Henshaw · B. A. Perdue · R. M. Prior · P.-N. Seo · S. Stave · H. R. Weller

Received: 17 August 2011 / Accepted: 1 October 2011 / Published online: 21 October 2011

Abstract Measurements of the absolute cross section and angular distributions for the $^{11}B(p,\alpha)^{8}Be \rightarrow \alpha + \alpha$ and the $^{11}B(\alpha,\alpha)^{11}B$ reactions have been performed from 0.15 to 3.8 MeV for the $^{11}B(p,\alpha)$ study and from 2 to 5.4 MeV for the $^{11}B(\alpha,\alpha)$ reaction. The absolute cross sections are presented in terms of the total number of α-particles detected in order to avoid uncertainties due to ambiguities in the number of alpha particles emitted in the reaction at a particular energy. The angular distributions of the $^{11}B(p,\alpha)^{8}Be(2^{+})$ reaction were fit to a Legendre polynomial expansion and the coefficients are presented. Finally, the $^{11}B(\alpha,\alpha)^{11}B$ data were fit in terms of phase shifts (ignoring the spin of the target), providing a convenient representation of the elastic cross section data between 2 and 5.4 MeV.

Keywords Low energy nuclear physics · Aneutronic fusion · Fusion · Triple alpha · Energy production · ^{11}B · Alpha · Proton fusion · Alpha elastic scattering · Cross section · Angular distribution

Introduction

As previously discussed [1], the history of the study of the $^{11}B(p,\alpha)$ reaction is almost as long as the history of nuclear physics itself. This reaction was studied and discussed in some detail by Oliphant and Rutherford [2] almost 80 years ago for proton energies around 200 keV. At that time there was a considerable controversy as to whether the most probable mode of emission of the three α-particles was with equal energies at 120° with respect to each other, or with two particles emitted back to back, while the third remained almost at rest. Three years after the paper by Oliphant and Rutherford, who subscribed to the first interpretation, Dee and Gilbert [3], also of the Cavendish Laboratory, published results concluding that at $E_p = 300$

Electronic supplementary material The online version of this article (doi:10.1007/s10894-011-9473-5) contains supplementary material, which is available to authorized users.

M. C. Spraker (✉) · R. M. Prior
North Georgia College and State University,
Dahlonega, GA, USA
e-mail: mcspraker@northgeorgia.edu

M. W. Ahmed · M. A. Blackston · N. Brown ·
S. S. Henshaw · B. A. Perdue · S. Stave · H. R. Weller
Duke University and TUNL, Durham, NC, USA

Present Address:
M. W. Ahmed
North Carolina Central University, Durham, NC 27707, USA

Present Address:
M. A. Blackston
Oak Ridge National Laboratory, Oak Ridge, TN, USA

R. H. France III
Georgia College and State University, Milledgeville, GA, USA

Present Address:
B. A. Perdue
Los Alamos National Laboratory, Los Alamos, NM, USA

P.-N. Seo
University of Virginia and TUNL, Charlottesville, VA, USA

Present Address:
S. Stave
Pacific Northwest National Laboratory, Richland, WA, USA

keV, "the common mode of disintegration is into two [alpha] particles which proceed at angles of 150° to 180° relatively to one another, the third particle receiving very little energy".

This reaction has been studied numerous times over the intervening years [4]. The modern view of this reaction is contained in Ref. [5] which contains references to many previous studies. This paper discussed data from $E_{cm} = 22$ to 1100 keV. It claimed that the reaction proceeded predominantly by a sequential decay through the ground and first excited states of ^{8}Be over the entire energy range and maintained that the 2^- resonance at E_p = 0.675 MeV decayed via a two-step sequential process which proceeded via $\ell = 1$ α-particles leading to the 2^+ first excited state of ^{8}Be. The subsequent decay of this state would then produce two secondary α-particles. According to their simulation, the α-particle yield consisted of one high energy (≈4 MeV) primary α-particle and a secondary α-particle yield peaked at an energy just below 1 MeV with an intensity about equal to the primary α-particle yield as shown in Ref. [5]. The present data and simulations disagree with these conclusions at the 0.675 MeV 2^- resonance. A previous interpretation of this reaction [6], which is not discussed in Ref. [5], also found that the two-step model with $\ell = 1$ primary α-particles failed to describe the data at the 2^- resonance. However, they found that they could describe the data at the 0.675 MeV resonance by assuming that the primary α-particle decayed with $\ell = 3$ as confirmed in Ref. [1].

From an astrophysical point of view, the ^{11}B(p,α) reaction is interesting because it is the primary pathway for depleting ^{11}B in stellar interiors. The abundance of ^{11}B observed in stellar atmospheres can be used to determine the depth of stellar convection when studied in comparison to the abundances of Li and Be [7].

In addition, one of the more serious problems in developing practical nuclear fusion power involves reactor activation by the high flux of neutrons from standard fusion fuels (e.g. ^{3}H(d,n)α). There is interest in developing advanced aneutronic fusion fuels such as ^{11}B which undergoes fusion via the ^{11}B(p,α)αα reaction. Harnessing such a process may be possible with advanced non-equilibrium colliding beam reactors [8]. The three α-particles produced in this reaction range in energy up to around 5.4 MeV. It is important for the design and simulations of such a reactor to know the number of α-particles as a function of proton and α-particle energy. One goal of the present experiment was to provide complete and accurate data for this purpose. The non-thermal α-particles can then undergo reactions with other ^{11}B nuclei in the reactor. With this in mind, the second portion of this paper will present the experimental results on the cross sections of the ^{11}B(α,α)^{11}B reaction from 2 to 5.4 MeV.

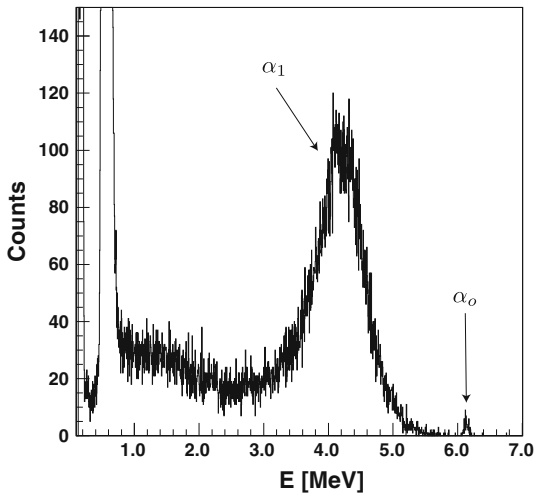

Fig. 1 Raw data spectrum taken at 90° on the 0.675 MeV resonance. The α_0 and α_1 peaks are clearly visible. The large peak just below 1 MeV is produced by elastically scattered protons

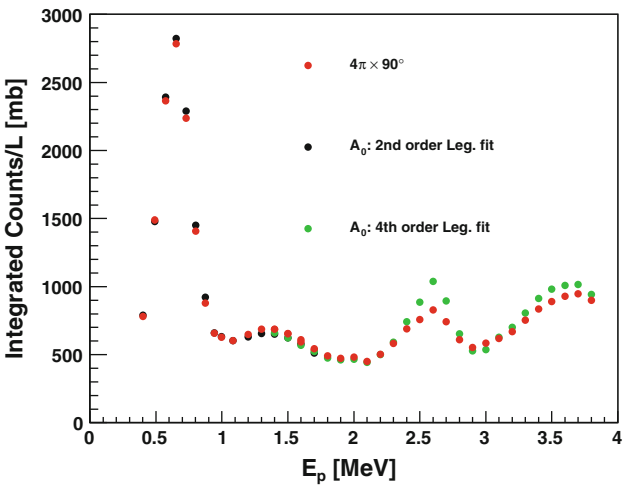

Fig. 2 Comparison of the integrated Counts/$Ld\Omega$ and the Legendre polynomial fits. The Legendre fits are shown using the *Black* and *Green dots*. While the resonance at 0.675 MeV exhibits isotropy, anisotropy can be seen for the resonance at 2.64 MeV for the $^{11}\mathrm{B}(p,\alpha)^{8}Be \rightarrow \alpha + \alpha$ data. The *statistical errors* are smaller than the *plotted circles*

^{11}B(p,α)αα

The measurements were performed at the Triangle Universities Nuclear Laboratory (TUNL). Both the TUNL FN Tandem Van de Graaff and Mini-Tandem accelerators were used. The ^{11}B(p,α) data were taken in a series of experiments in which the proton energy ranged from 0.15–0.4, 0.4–1.7 to 1.4–3.8 MeV. The lowest energy data were taken using the TUNL Mini-Tandem. Energies around the E_p = 0.675 MeV resonance from 401 keV to 1.08 MeV were studied using proton beams of incident energy from 1.20 MeV through 1.65 MeV in 50 keV steps

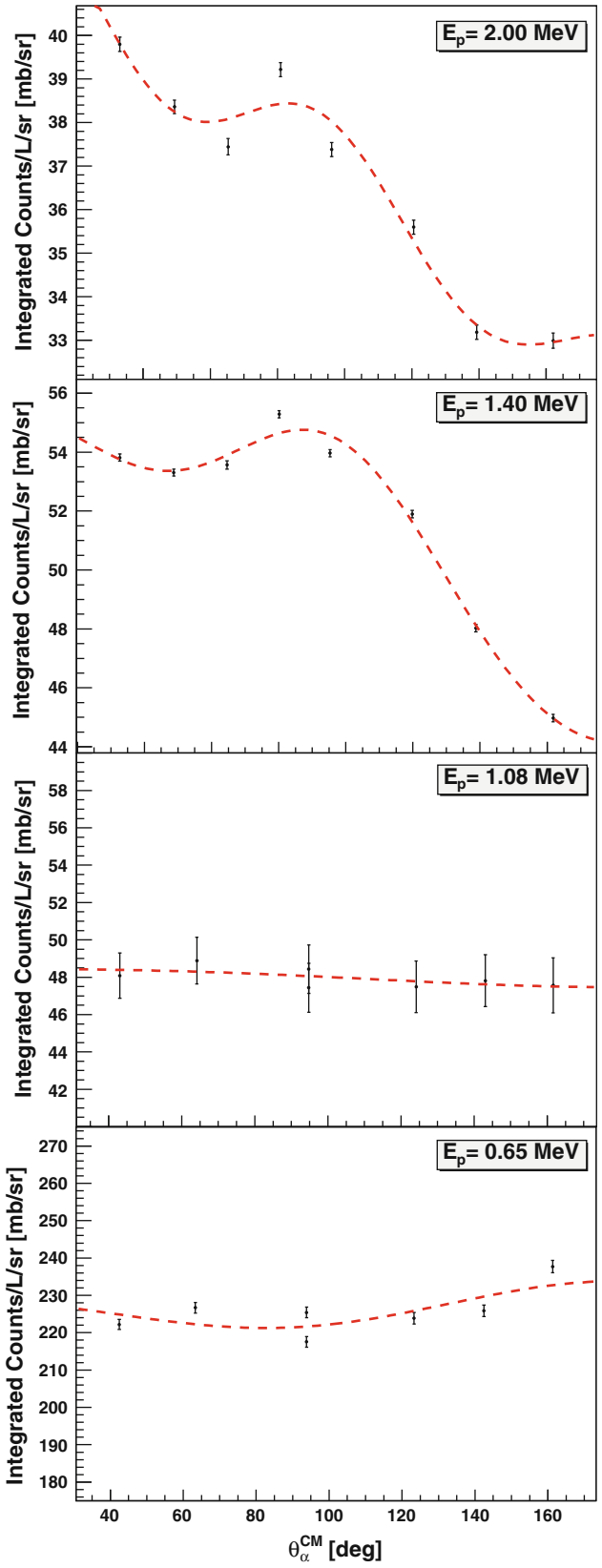

Fig. 3 ^{11}B(p,α) data and the associated Legendre polynomial fits (*dashed lines*) at selected energies. The errors shown are statistical only

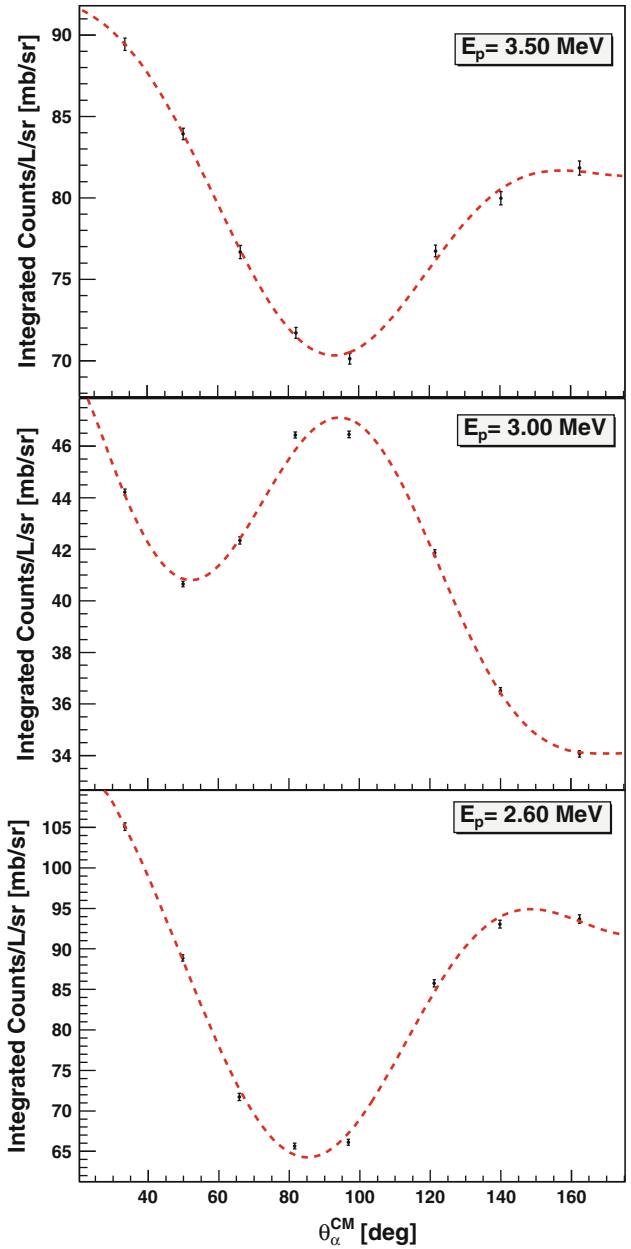

Fig. 4 ^{11}B(p,α) data and the associated Legendre polynomial fits (*dashed lines*) at selected energies. The *errors* shown are statistical only

passing through a standard commercial aluminum foil used as a beam degrader. At these energies beam intensities varied from 0.5 to 10 nA on target and beam resolution varied from approximately 60 to 70 keV. For the other two measurements, beam intensities in the 100 to 200 nA range were used.

The outgoing α-particles were detected by eight silicon surface barrier detectors with sufficient thickness to stop the α-particles at all energies. A typical spectrum at the 0.675 MeV resonance measured at 90° is shown in Fig. 1. The detectors were located 16.5 cm from the target, which

Table 1 Results of the 2nd order Legendre polynomial fitting integrated α_1 Counts/$Ld\Omega$ data covering the incident proton energy range of 0.15 up to 1.3 MeV

E (MeV)	A_0 (mb/sr)	A_1 (mb/sr)	A_2 (mb/sr)
0.15	0.91 ± 0.015	0.023 ± 0.033	−0.011 ± 0.041
0.22	5.815 ± 0.045	−0.272 ± 0.097	−0.14 ± 0.12
0.25	9.307 ± 0.065	0.019 ± 0.14	−0.05 ± 0.18
0.30	20.837 ± 0.092	−0.35 ± 0.20	−0.73 ± 0.25
0.40	61.85 ± 0.43	−0.03 ± 0.93	0.46 ± 1.16
0.40	61.85 ± 0.42	1.04 ± 0.77	0.13 ± 0.99
0.49	114.01 ± 0.88	1.13 ± 1.60	−1.27 ± 2.07
0.57	187.84 ± 0.68	−1.19 ± 1.24	3.44 ± 1.60
0.65	218.42 ± 0.55	−3.17 ± 1.00	6.31 ± 1.30
0.73	179.73 ± 0.50	−3.86 ± 0.91	8.84 ± 1.17
0.80	112.20 ± 0.35	−5.40 ± 0.65	8.07 ± 0.84
0.88	72.44 ± 0.30	−3.11 ± 0.55	6.76 ± 0.72
0.94	51.25 ± 0.24	1.57 ± 0.43	0.17 ± 0.56
1.00	48.78 ± 0.35	2.01 ± 0.65	0.28 ± 0.84
1.08	47.36 ± 0.51	0.34 ± 0.92	−0.15 ± 1.19
1.20	49.39 ± 0.11	0.22 ± 0.21	−3.60 ± 0.27
1.30	50.63 ± 0.09	0.55 ± 0.15	−5.34 ± 0.20

The uncertainties are statistical only

was composed of 56 ± 2 μg/cm^2 of isotopically pure ^{11}B deposited on a 9 μg/cm^2 carbon backing. Target thickness was measured using elastically scattered α-particles at 4.86 MeV, where the ratio of the elastic scattering cross section to the purely electromagnetic Rutherford cross section is known at a scattering angle of 165° [9]. This measurement provided two independent measures of the target thickness *via* the known cross section and via the energy loss as measured by the broadening of the elastic peak. Analyses of both results agree and provide a target thickness of 56 ± 2 μg/cm^2 leading to a 3.6% systematic uncertainty in our yields.

The relative solid angles for each detector were measured using low energy Rutherford scattering on gold as well as a known ^{241}Am source. The data were normalized by the integrated beam current and the detector solid angles. Detectors were placed at $\theta_\alpha^{lab} = 30°, 45°, 60°, 75°, 90°, 115°, 135°$, and 160°, with each detector subtending a solid angle of approximately 2.5 × 10^{-4} sr.

Although three α-particles are emitted in this reaction, the number of α-particles in a given energy interval depends upon the details of the reaction dynamics. As is shown in Ref. [1], the energy distribution of the secondary

Table 2 Results of the 4th order Legendre polynomial fitting of the integrated α_1 Counts/$Ld\Omega$ data covering the incident proton energy range from 1.4 to 3.8 MeV

E (MeV)	A_0 (mb/sr)	A_1 (mb/sr)	A_2 (mb/sr)	A_3 (mb/sr)	A_4 (mb/sr)
1.40	52.46 ± 0.046	3.69 ± 0.077	−3.79 ± 0.10	1.84 ± 0.14	1.03 ± 0.15
1.50	49.68 ± 0.045	3.99 ± 0.076	−3.87 ± 0.10	1.86 ± 0.14	0.10 ± 0.15
1.60	45.34 ± 0.049	4.24 ± 0.082	−3.31 ± 0.11	2.04 ± 0.15	0.91 ± 0.16
1.70	41.64 ± 0.036	4.04 ± 0.061	−2.64 ± 0.083	2.06 ± 0.11	1.05 ± 0.12
1.80	37.90 ± 0.039	4.23 ± 0.066	−1.49 ± 0.091	2.38 ± 0.12	1.31 ± 0.13
1.90	36.67 ± 0.055	4.16 ± 0.093	−0.93 ± 0.13	2.57 ± 0.17	1.67 ± 0.18
2.00	37.13 ± 0.061	3.74 ± 0.10	−0.95 ± 0.14	1.23 ± 0.19	1.95 ± 0.20
2.10	35.24 ± 0.042	3.82 ± 0.072	0.68 ± 0.098	3.61 ± 0.13	2.85 ± 0.14
2.20	39.78 ± 0.055	3.51 ± 0.095	1.94 ± 0.13	5.49 ± 0.17	4.29 ± 0.18
2.30	47.09 ± 0.071	3.78 ± 0.12	5.12 ± 0.17	8.27 ± 0.23	6.01 ± 0.24
2.40	58.98 ± 0.11	3.61 ± 0.19	13.06 ± 0.25	11.32 ± 0.34	7.55 ± 0.35
2.50	70.41 ± 0.14	3.11 ± 0.25	23.16 ± 0.33	13.59 ± 0.44	3.80 ± 0.46
2.60	82.63 ± 0.16	3.53 ± 0.29	30.33 ± 0.38	10.77 ± 0.50	−7.14 ± 0.53
2.70	71.20 ± 0.13	3.58 ± 0.24	16.39 ± 0.32	3.74 ± 0.43	−14.18 ± 0.45
2.80	51.92 ± 0.089	3.70 ± 0.16	0.94 ± 0.21	2.15 ± 0.29	−9.25 ± 0.30
2.90	41.91 ± 0.14	3.85 ± 0.23	−5.75 ± 0.31	2.73 ± 0.43	−2.02 ± 0.45
3.00	42.74 ± 0.046	3.99 ± 0.077	−4.45 ± 0.11	5.49 ± 0.14	5.29 ± 0.15
3.10	49.90 ± 0.059	4.25 ± 0.10	5.22 ± 0.14	5.63 ± 0.19	6.15 ± 0.20
3.20	55.69 ± 0.082	4.90 ± 0.15	7.37 ± 0.20	5.72 ± 0.26	3.27 ± 0.27
3.30	64.19 ± 0.076	4.65 ± 0.14	8.85 ± 0.18	4.71 ± 0.25	−0.37 ± 0.26
3.40	72.66 ± 0.073	5.11 ± 0.13	10.68 ± 0.18	3.66 ± 0.24	−3.64 ± 0.25
3.50	78.11 ± 0.14	4.72 ± 0.25	12.57 ± 0.33	0.87 ± 0.44	−3.79 ± 0.46
3.60	80.22 ± 0.067	5.74 ± 0.12	7.52 ± 0.16	0.64 ± 0.22	−9.46 ± 0.22
3.70	80.76 ± 0.062	6.87 ± 0.11	5.05 ± 0.15	0.85 ± 0.20	−10.46 ± 0.21
3.80	74.92 ± 0.060	6.51 ± 0.11	1.97 ± 0.14	0.70 ± 0.20	−9.13 ± 0.20

The uncertainties are statistical only

α-particles varies with proton energy. This leads to a different number of α-particles in a given outgoing α-particle energy bin. For the energy range used to generate the angular distributions in this paper (a 2.75 MeV wide α-particle energy bin centered on the centroid of the dominant α-particle peak), simulations show that out of the three emitted α-particles, on average 2.1 α-particles contribute to this peak at the 0.675 MeV resonance compared to only about 1.5 α-particles for the 2.64 MeV resonance. To avoid the model dependence associated with the determination of the value of the number of α-particles and to provide useable results that can be compared to other data, this study will report the Counts/Luminosity, X, where X is defined by the following equation:

$$X = \frac{\text{Counts}}{N_t N_p d\Omega}(\text{cm}^2/\text{sr}) \tag{1}$$

where N_t is the number of target ^{11}B nuclei per cm^2, N_p is the number of incident protons, and $d\Omega$ is the solid angle of the detector. The luminosity (L) is defined to be equal to $N_p \times N_t$. X has the same units as a differential cross section but with an important difference: the expected number of α-particles has not been divided out. This quantity, X, describes the total number of detected outgoing α-particles in the reaction.

To demonstrate the usefulness of X, the number of α-particles will be calculated for a simple example. Assume one incident proton per second interacts with a target of one ^{11}B nucleus per square centimeter. The X quantity at $E_p = 1.4$ MeV for the 90° detector in the E_α bin centered at 4.635 MeV (4.59 MeV $\leq E_\alpha \leq$ 4.68 MeV) is 4.28 mb/sr. See Fig. 5 or the appended table. Assuming isotropy, and integrating over all angles (4π) yields an α-particle rate between 4.59 and 4.68 MeV of:

$$4.28\text{mb/sr} \times 1/s \times 1/\text{cm}^2 \times 4\pi\text{sr} \times (1 \times 10^{-27}\text{cm}^2/\text{mb}) = 5.38 \times 10^{-26}/\text{s}. \tag{2}$$

Of course, during the actual experiment the number of protons was about 200 nA (1.25×10^{12} protons/s) with 3×10^{18} ^{11}B target nuclei per square centimeter. Under these conditions, approximately 2×10^5 α-particles per second are produced between 4.59 and 4.68 MeV.

The measured $X = \text{Counts}/Ld\Omega$ was integrated in two different ways. In the first method, X was integrated over the α-particle center-of-mass energy in a 2.75 MeV wide region centered on the α_1 peak (Note that the α_1 reaction channel corresponds to the channel in which the ^8Be nucleus is left in its first excited state while for the α_0 channel, the ^{8}Be is left in its ground state). The measured angular dependence of the energy integrated X in the center-of-mass frame was fit with a Legendre polynomial expansion up to order l using a Minuit χ^2 minimization technique:

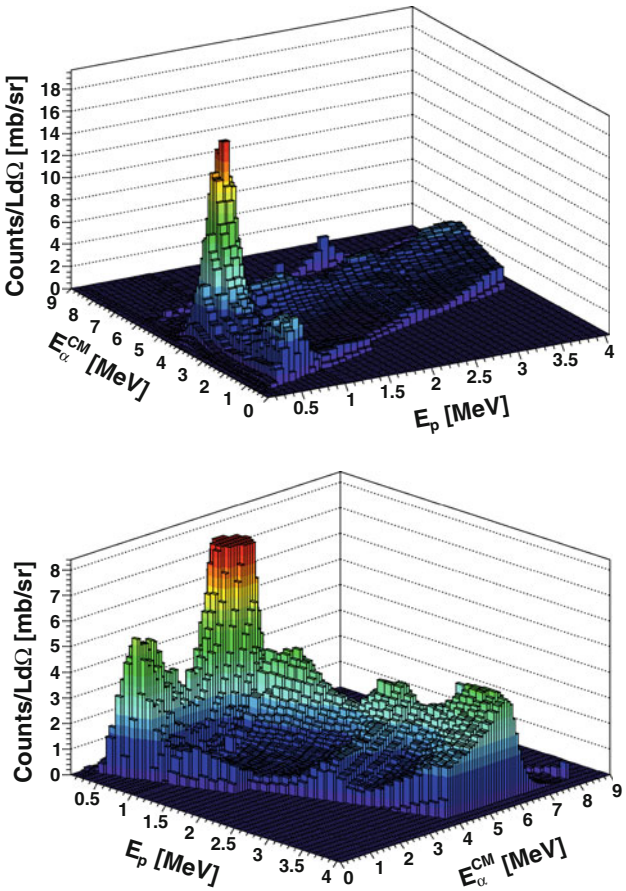

Fig. 5 Distribution of Counts/$Ld\Omega$ vs. E_α^{CM} and E_p at $\theta_{lab} = 90°$ over the initial proton energy range from 0.15 MeV to 3.8 MeV. The *top* figure shows the full range of the z-axis. The *bottom* figure is the same as the top but rotated and with a rescaled z-axis to emphasize the structure observed at higher energies. The *statistical errors* are given in the appended tables

$$\frac{d\sigma(\theta)}{d\Omega} \propto X(\theta) = \sum_{i=0}^{i=l} A_i P_i(\cos\theta). \tag{3}$$

The A_0 term of the expansion was then multiplied by 4π to yield the total integrated Counts/L for each incident beam energy.

In the second approach, X in the center-of-mass frame for the $\theta_\alpha^{lab} = 90°$ detector was integrated over the same α-particle energy region and multiplied by 4π to yield the total integrated Counts/L. If the angular distribution is truly isotropic, these two methods will yield the same result. If they differ, then it allows us to quantify the amount that the cross section deviates from an isotropic one. The results of this study are shown in Fig. 2. For the energy range ($E_p = 0.4$–1.2 MeV), the two integration methods deviate by no more than 3% indicating that the α-particle angular distributions are very nearly isotropic. However, in the overlapping energy range ($E_p = 1.4$–1.7 MeV) the two

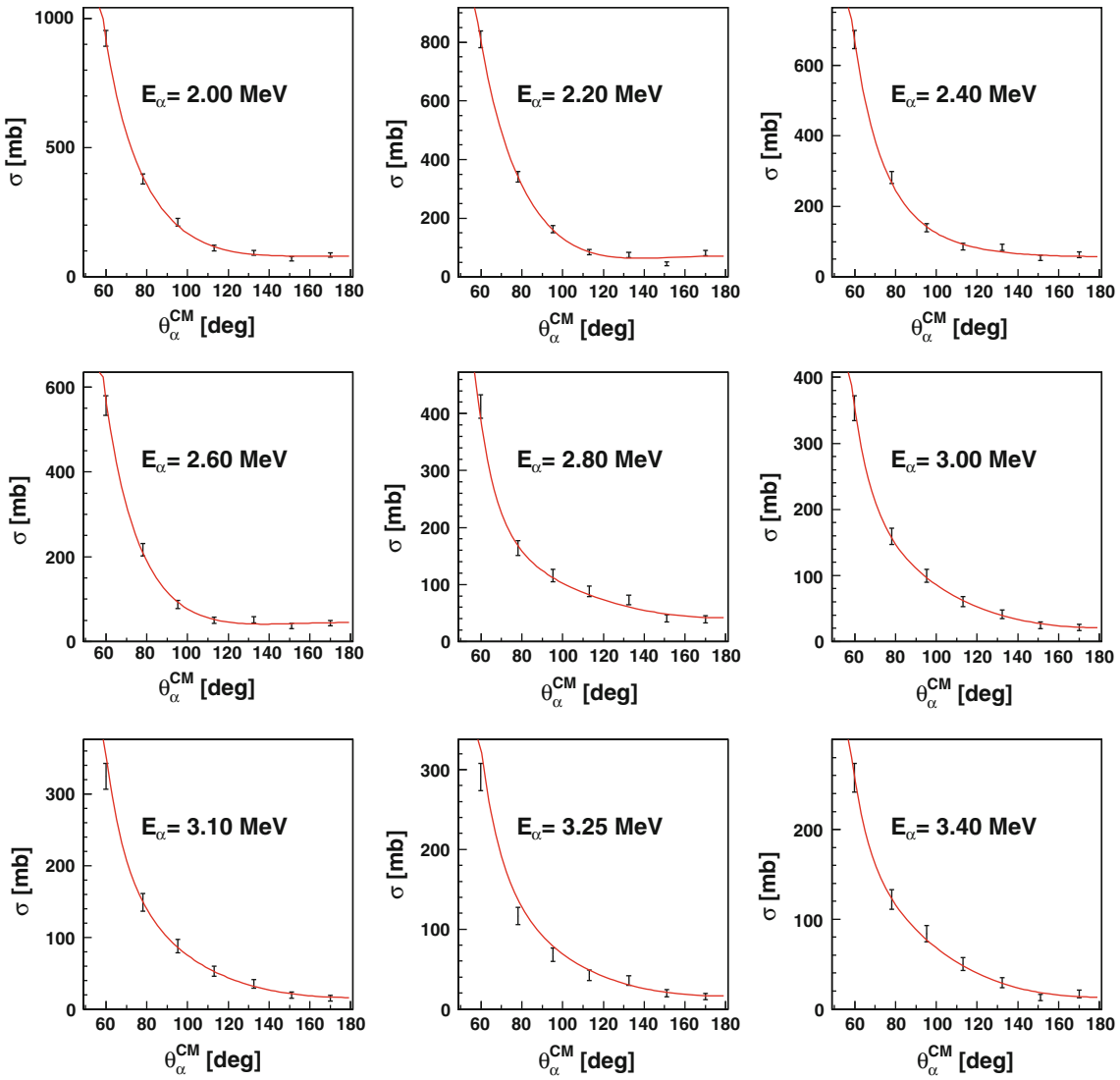

Fig. 6 2.00 - 3.40 MeV ^{11}B(α,α)^{11}B elastic scattering data plotted against the phase shift analysis fits (*solid line*). All *errors* shown are statistical

methods start to differ more but only by about 5%. In the higher energy region the ratio differs from 1.0 by up to 25% near $E_p = 2.6$ MeV but is very close to 1.0 in other regions.

Whereas the resonance at 0.675 MeV is $J^\pi = 2^-$, the resonance at 2.64 MeV is $J^\pi = 3^-$. Angular momentum formalism and a two-step reaction model lead to an expectation of an isotropic distribution at $E_p = 0.675$ MeV and an anisotropic distribution for the $E_p = 2.64$ MeV 3^- resonance (see Ref. [1]), both of which are confirmed by the present and past experiments (Refs. [1, 10]).

In addition to determining the deviation from isotropy, the coefficients of the Legendre polynomial fits can be used to smoothly evaluate the Counts/($Ld\Omega$) at any angle. The Legendre polynomial fits represent the data extremely well with over 97% of the data being within 3% of the fitted values. Figures 3 and 4 show the experimental data and the associated fits at energies both on and off the resonances. The numerical values for the fit parameters along with their uncertainties are shown in Tables 1 and 2.

Figure 5 shows the distribution of Counts/$Ld\Omega$ versus E_α^{CM} and E_p at $\theta_{lab} = 90°$ over the entire range of initial proton energies. The resonance near $E_p = 0.675$ MeV is clearly visible with α-particle energies near 4 MeV. The α_0 peaks are just visible in this plot and are at about 6 MeV and higher. The resonances at incident proton energies of 1.388, 2.64 and 3.5 MeV are visible but not distinct on this scale. The bottom plot in Fig. 5 is the same as the top figure but rotated and with a rescaled z-axis that emphasizes the structures seen at the higher proton energies.

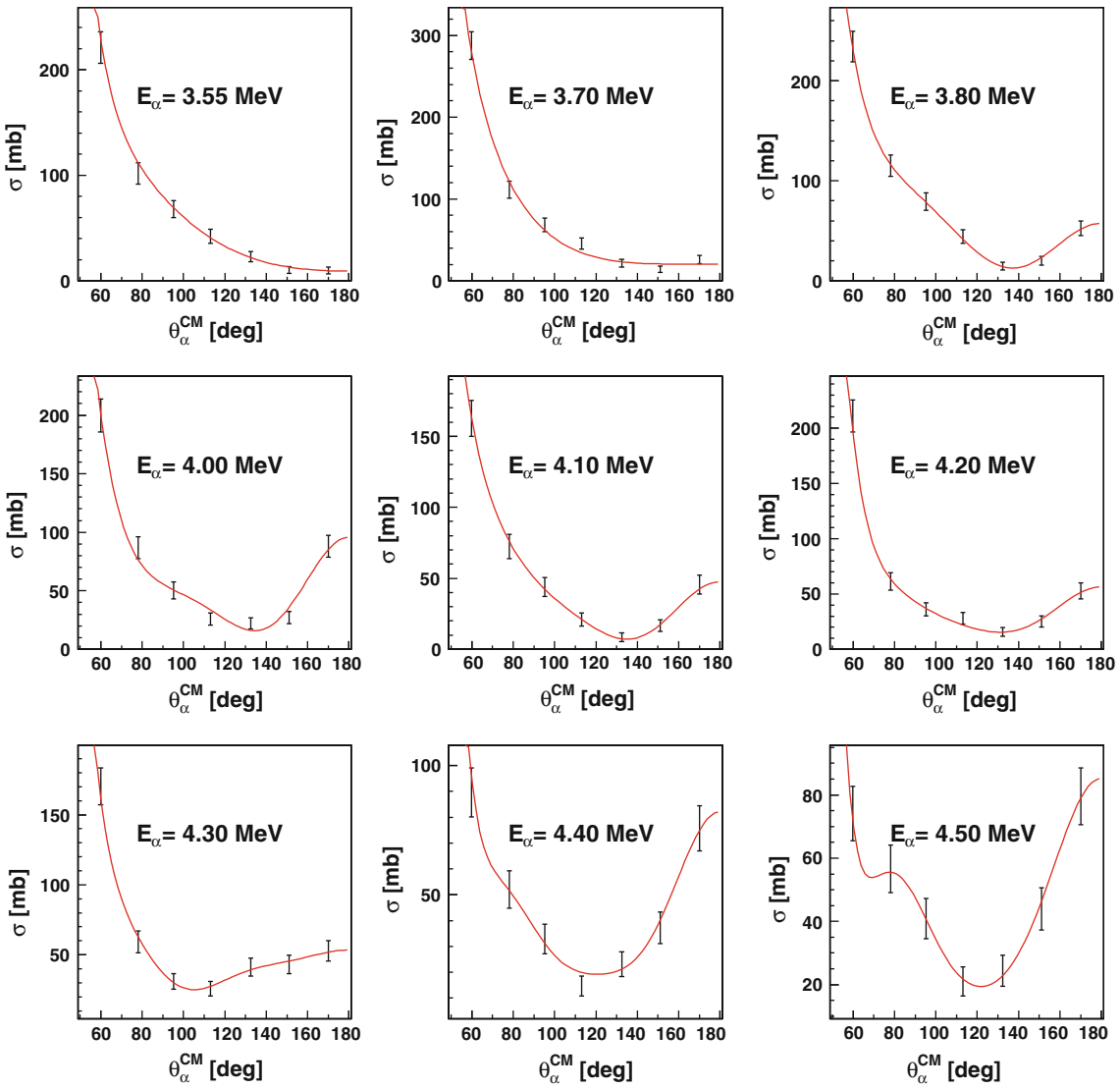

Fig. 7 3.55–4.50 MeV ^{11}B(α,α)^{11}B elastic scattering data plotted against the phase shift analysis fits (*solid line*). All *errors* shown are statistical

^{11}B(α,α)^{11}B

The ^{11}B(α,α)^{11}B reaction was studied using the previously described experimental setup and ≈10 nA incident α-particle beams. Elastic scattering from a 105 μg/cm^2 Au target was used to provide Rutherford scattering to calibrate the relative solid angles of the detectors. The absolute elastic scattering cross section from ^{11}B was extracted with an estimated systematic error of ±5% using the fact that the cross section is given by pure Rutherford scattering at low energies and small angles. A ^{12}C target was used to remove carbon generated events from the ^{11}B target, which was composed of 76 μg/cm^2 of isotopically pure ^{11}B sandwiched between layers of 20 and 46 μg/cm^2 Ti. Since the elastic scattered α-particle events from ^{11}B and ^{12}C could be separated at backward angles, full ^{12}C angular distrubutions made it possible to unfold the ^{12}C generated events at all angles.

An exact phase-shift analysis of the elastic scattering data would be complicated by the 3/2 spin of the ^{11}B nucleus, and would require additional data at each energy because of the larger number of partial waves that would have to be included. Physically, the spin of the target nucleus is not likely to have much effect on the angular dependence of the cross section, so a simpler formalism, using phase shifts for spin-0 particles scattering from a spin-0 target, was used to fit the data. Since the main objective of this analysis is to provide a convenient parametrization of the cross section data for the purpose of representing the data at all angles and energies (within the

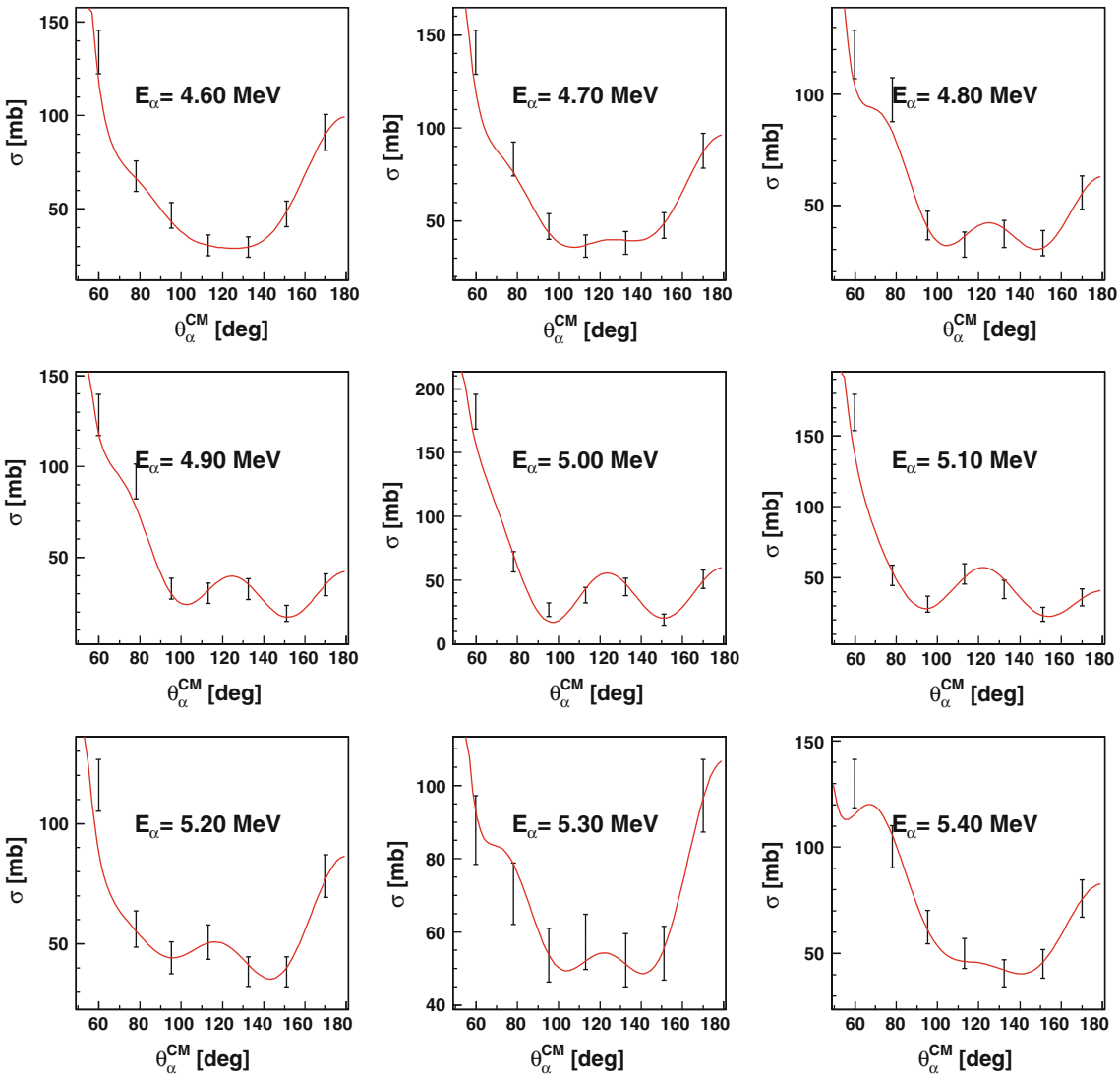

Fig. 8 4.60–5.40 MeV ^{11}B(α,α)^{11}B elastic scattering data plotted against the phase shift analysis fits (*solid line*). All *errors* shown are statistical

range of this experiment), this simplification should be more than adequate and will be tested by its ability to reproduce the measured values. The formalism is given below.

The differential cross section can be written in terms of two complex scattering amplitudes, F_C and F_N:

$$\frac{d\sigma}{d\Omega}(\theta) = \frac{1}{k^2}|F_C + F_N|^2 \tag{4}$$

where the wave number $k = 0.2187 \times 10^{13}\mu\sqrt{\frac{E}{m_1}}\text{cm}^{-1}$ for E in MeV and m_1 in amu. The quantity μ is the reduced mass $\mu = \frac{m_1 m_2}{m_1+m_2}$. The terms m_1 and m_2 are the incident and target particle masses, respectively. The Coulomb scattering amplitude F_C is written in terms of the center-of-mass scattering angle θ and the quantity η as:

$$F_C = -\frac{1}{2}\eta\left(\frac{1}{\sin^2(\frac{\theta}{2})}\right)e^{i\eta\ln\left(\frac{1}{\sin^2(\frac{\theta}{2})}\right)}, \tag{5}$$

where $\eta = \frac{Z_1 Z_2}{\hbar v} = 0.1575 Z_1 Z_2\sqrt{\frac{m_1}{E}}$ (E in MeV and v is the velocity in the lab frame). The terms Z_1 and Z_2 are the incident and target particle atomic numbers, respectively. The nuclear scattering amplitude F_N is:

$$F_N = -\frac{i}{2}\sum_{l=0}^{l_{max}} e^{i\alpha_l}(2l+1)(S_l - 1)P_l(\cos\theta) \tag{6}$$

where the Coulomb phase shift is given by $\alpha_0 = 0, \alpha_l = \alpha_{l-1} + 2\tan^{-1}\left(\frac{\eta}{l}\right)$ and $S_l = \gamma_l e^{2i\delta_l}$. The parameters that have to be determined to reproduce the experimental cross section data are δ_l, the real part of the phase shift, and γ_l, the damping parameter that represents the

Table 3 The phase shifts and damping parameters resulting from fitting the $^{11}B(\alpha,\alpha)$ data between 2 and 5.4 MeV

E (MeV)	δ_0 (deg)	δ_1 (deg)	δ_2 (deg)	δ_3 (deg)	γ_0	γ_1	γ_2	γ_3
2.00	−6.65	−7.49	0.00	0.00	1.00	0.81	1.00	1.00
2.20	−2.97	−12.52	0.00	0.00	1.00	0.77	1.00	1.00
2.40	−4.40	−3.12	0.00	0.00	1.00	1.00	1.00	1.00
2.60	1.01	−7.08	0.00	0.00	0.63	0.83	1.00	1.00
2.80	−18.55	4.73	0.00	0.00	1.00	1.00	1.00	1.00
3.00	−8.79	7.69	0.00	0.00	1.00	0.96	1.00	1.00
3.25	−1.11	6.77	0.00	0.00	1.00	1.00	1.00	1.00
3.40	−12.79	9.17	0.00	0.00	1.00	0.88	1.00	1.00
3.55	−6.81	14.65	0.00	0.00	1.00	0.92	1.00	1.00
3.70	−10.31	−7.61	0.00	0.00	1.00	0.73	1.00	1.00
3.85	−16.28	−18.99	−5.59	4.43	1.00	0.47	1.00	1.00
4.00	−10.93	−20.54	3.95	9.62	1.00	0.52	1.00	1.00
4.10	−23.71	11.58	−4.42	−4.70	1.00	0.52	0.53	0.98
4.20	50.79	−7.94	−25.82	−8.34	1.00	0.73	1.00	1.00
4.30	64.66	−17.56	−21.11	−9.07	1.00	0.38	1.00	1.00
4.40	69.67	24.54	−23.88	−10.95	1.00	0.53	0.87	1.00
4.50	75.54	30.12	−28.10	−10.22	1.00	0.46	0.84	0.93
4.60	60.88	3.87	−32.47	−14.10	1.00	0.40	1.00	1.00
4.70	61.24	2.36	−34.38	−17.56	1.00	0.30	1.00	1.00
4.80	67.34	9.93	−31.53	−20.63	1.00	0.37	1.00	0.99
4.90	59.51	−1.97	−29.55	−21.73	1.00	0.49	1.00	1.00
5.00	44.50	−29.74	−32.92	−23.45	1.00	0.27	0.73	1.00
5.10	55.14	−38.69	−34.45	−18.32	1.00	0.40	0.74	1.00
5.20	68.41	27.55	−39.00	−16.44	1.00	0.00	0.74	1.00
5.30	66.41	58.55	−41.43	−19.83	1.00	0.00	0.97	1.00
5.40	105.48	80.49	−36.44	−15.38	1.00	0.67	0.69	1.00

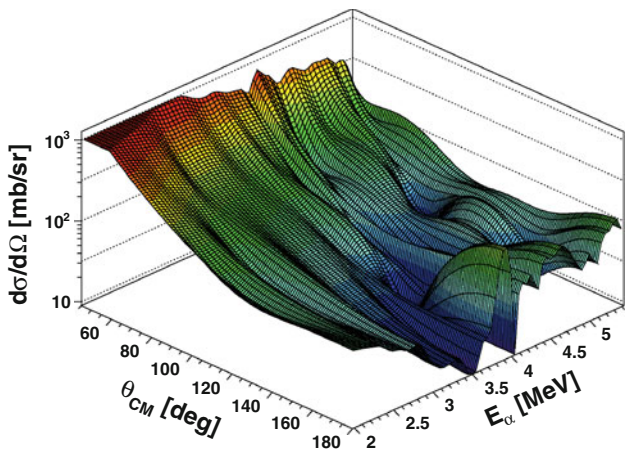

Fig. 9 The differential cross section evaluated using the fitted phase shifts for the $^{11}B(\alpha,\alpha)^{11}B$ reaction for incident α-particle energies between 2 and 5.4 MeV as a function of the outgoing α-particle polar angle in the center-of-mass frame

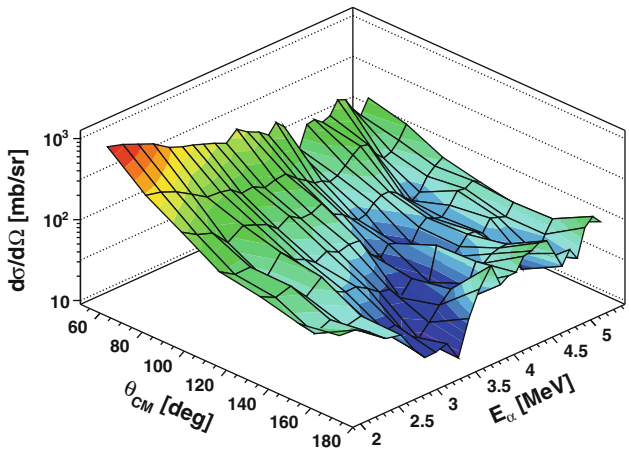

Fig. 10 The experimentally determined differential cross section for the $^{11}B(\alpha,\alpha)^{11}B$ reaction for incident α-particle energies between 2 and 5.4 MeV as a function of the outgoing α-particle polar angle in the center-of-mass frame. The statistical uncertainty can be seen in Figs. 6, 7 and 8

imaginary part of the phase shift for each l-value included in the fit. The real part of the phase shift is expressed in degrees. The damping parameter represents absorption of the corresponding partial wave; it is dimensionless and varies between 1.0 (meaning no absorption) and 0 (meaning total absorption).

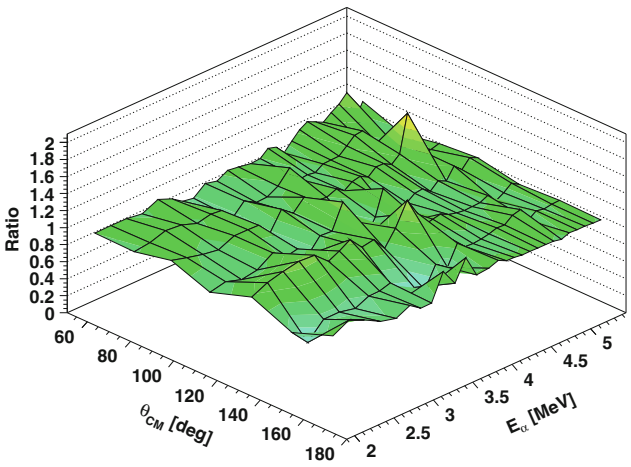

Fig. 11 The ratio of the data shown in Fig. 10 to the cross section calculated using the results of the phase-shift fit for the ^{11}B(α,α)^{11}B reaction. The agreement is excellent. The ratio has a value of 1.015 ± 0.114 averaged over the data in the plot

No attempt has been made to interpret the analysis in terms of the reaction mechanism. The results provide a way to parametrize the entire data set and allow interpolation over energies within the range of the data and to interpolate and extrapolate to any scattering angle.

Partial waves for angular momentum quantum numbers 0 through 3 were included in this analysis, meaning four complex phase shifts were adjusted. Since each phase shift is a complex number, two parameters were adjusted for each phase shift giving a maximum of 8 parameters. At the lower energies the higher order phase shifts were not needed so that fewer parameters had to be determined. The fitting was done with a Fortran code that used the Marquart method [11] for determining the parameters.

The angular distribution data at energies from 2.0 to 5.4 MeV were transformed into the center-of-mass system and then fit at each energy. The data and the accompanying fits are shown in Figs. 6, 7, and 8. Tables of phase shifts and damping parameters (see Table 3) can then be used to calculate cross sections at any energy between 2.0 and 5.4 MeV by interpolating the table of fitted parameters and using the parameters to calculate the corresponding cross section. The cross sections can also be calculated at any angle between 0° and 180°. Figure 9 shows the calculated cross section as a function of angle and energy over the range from 2.0 to 5.4 MeV. Over 90% of the fitted differential cross section values are within 20% of the experimental input data. To demonstrate this good agreement, two additional plots are included. The first is Fig. 10 which shows the measured differential cross section as a function of incident α-particle energy and outgoing α-particle polar angle in the center-of-mass frame. The coarseness is due to the finite number of angles at which the cross section was measured as well as the finite number of incident α-particle energies used. These are the data that were fit with the phase shift analysis. The ratios of the measured cross sections to the values calculated using the phase shifts in Table 3 are shown in Fig. 11. It is clear that the fits are very good and that the phase shifts provide a convenient and accurate representation of the data.

Conclusion

This paper has reported the results of measurements which determined the absolute values of the total number of outgoing α-particles from the $^{11}\mathrm{B}(p,\alpha)^{8}Be \rightarrow \alpha + \alpha$ reaction for E_p between 0.15 and 3.8 MeV as a function of the outgoing α-particle energy. The results at 90° are shown in Fig. 5; corresponding tabular results are appended. In addition, angular distributions of α-particles in a 2.75 MeV wide bin centered on the α_1 peak are presented at 42 energies between 0.15 and 3.8 MeV in the form of coefficients of Legendre polynomials which were fit to the data.

The overall systematic error on the absolute values of X reported in Fig. 5 is estimated as being ≤5%, arising primarily from the uncertainty in the target thickness. Statistical errors, although not shown in Fig. 5, are presented in the appended tables.

In addition, this paper has reported measurements of the angular distributions of the cross sections for the $^{11}\mathrm{B}(\alpha,\alpha)^{11}B$ elastic scattering reaction for incident E_α between 2 and 5.4 MeV. A phase shift analysis, using partial waves for the orbital angular momentum quantum numbers 0 through 3 and neglecting the spin of the target nucleus, was used to fit the data. Over 90% of the fitted differential cross section values were within 20% of the experimental input data. The systematic error is again dominated by the uncertainty in the target thickness and is estimated to be ≤5%. The statistical errors associated with the data points are presented in Figs. 6, 7, and 8. It is hoped that the data presented and tabulated in this paper will be useful to anyone designing a reactor, which incorporates the $^{11}\mathrm{B}(p,\alpha)^{8}Be \rightarrow \alpha + \alpha$ reaction in some manner.

Acknowledgments This work was supported in part by US Department of Energy grants DE-FG02-97ER41033 and DE-FG02-97ER41046 and Tri-Alpha Energy Incorporated.

References

1. S. Stave et al., Phys. Lett. B **696**, 26 (2011)
2. M. Oliphant, L. Rutherford, Proc. R. Soc. Lond. A **141**, 259 (1933)

3. P.I. Dee, C.W. Gilbert, Proc. R. Soc. Lond. A **154**, 279 (1936)
4. V.F.Dmitriev, arXiv.org nucl-th, 0812.2538v1 (2008).
5. H.W. Becker, C. Rolfs, H.P. Trautvetter, Z. Phys. A **327**, 341 (1987)
6. J. Quebert, L. Marquez, Nucl. Phys. A **126**, 646 (1969)
7. A.M. Boesgaard, C.P. Deliyannis, A. Steinhauer, Ap. J **621**, 991 (2005)
8. N. Rostoker, A. Qerushi, M. Binderbauer, J. Fusion Energ. **22**, 83 (2003)
9. J. Liu, Z.S. Zheng, W.K. Chu, Nucl. Instrum. Meth. B **108**, 1 (1996)
10. R.E. Segel, S.S. Hanna, R.G. Allas, Phys. Rev. **139**, B818 (1965)
11. D.W. Marquardt, J. Soc. Ind. Appl. Math. **11**(2), 431 (1963)